# Distributed Formal Analysis for Power Networks With Deep Integration of Distributed Energy Resources

Yan Li, Senior Member, IEEE, Peng Zhang , Senior Member, IEEE, Matthias Althoff, and Meng Yue, Member, IEEE

Abstract-A scalable distributed formal analysis (DFA) via reachable set computation is presented to efficiently evaluate the stability of large-scale interconnected power networks under heterogeneous disturbances induced by high penetration of distributed energy resources (DERs). Based on rigorous mathematical derivation, DFA is able to directly compute the boundaries of all possible dynamics and provide stability information, which is unattainable by traditional time-domain simulations or direct methods. An N+M decomposition approach is established to decouple a large-scale networked system and enable distributed reachable set calculations while also preserving the privacy of each subsystem. Numerical examples on a networked microgrid system show that DFA facilitates the efficient calculation and analysis of the impact DER disturbances can have on power network dynamics, which provides a potent means of optimizing the system's operation. Therefore, DFA provides an invaluable tool for designing and operating the interconnected power networks of the future, which will feature the deep integration of DERs.

*Index Terms*—Distributed formal analysis, reachable set, disturbances, stability, interconnected power networks, distributed energy resources (DERs).

#### I. INTRODUCTION

ISTRIBUTED energy resources (DERs) with coordinated management and interactive supports have demonstrated resiliency and reliability benefits to electricity customers [1]. However, the increased penetration of DERs in grids leads to new and unprecedented challenges as well [2], such as stability issues and coordination problems. Power electronic devices are usually used to interface DERs and other components (e.g., FACTS, energy storage systems, new type of loads, and HVDC

Manuscript received March 1, 2018; revised July 31, 2018; accepted September 24, 2018. Date of publication October 10, 2018; date of current version October 24, 2019. This work was supported in part by the National Science Foundation under Grants CNS-1647209 and ECCS-1611095, in part by the Department of Energy's Advanced Grid Modeling Program, in part by the Office of the Provost, University of Connecticut, and in part by the UTC Fellowship. Paper no. TPWRS-00298-2018. (Corresponding author: Peng Zhang.)

Y. Li and P. Zhang are with the Department of Electrical and Computer Engineering, University of Connecticut, Storrs, CT 06269 USA (e-mail: yan.7.li@uconn.edu; peng.zhang@uconn.edu).

M. Althoff is with the Department of Computer Science, Technische Universität München, Garching 85748, Germany (e-mail: althoff@tum.de).

M. Yue is with the Sustainable Energy Technologies Department, Brookhaven National Laboratory, Upton, NY 11973 USA (e-mail: yuemeng@bnl.gov).

Color versions of one or more of the figures in this paper are available online at http://ieeexplore.ieee.org.

Digital Object Identifier 10.1109/TPWRS.2018.2875150

links) with the grid. Although they enable ultra-fast grid control and load changes, the high penetration of power electronic components will reduce the grid inertia significantly, making the utility grid highly sensitive to disturbances [3] and threatening power system stability [4]. When the penetration level of DERs and microgrids is high, disturbances in the grid may trigger disconnections of a large number of DERs or microgrids within a short time window. This may pose a great threat to the bulk power system stability and security. Unfortunately, existing technologies have not been designed to address such issues.

Recently, formal analysis has emerged as an alternative and promising solution for the stability analysis of dynamic systems [5]–[8]. Formal analysis enables one to bound all system trajectories, which start from a set of unknown but bounded initial states, and simultaneously take into account the influence of uncertainties from parameters and/or inputs. The applications of formal analysis include, but are not limited to identifications of stability regions [5], control verification [6], [9], transient stability analysis [7], cyber-security [10], and load flow calculation [11].

Centralized formal analysis was discussed in [5], [12]. Specifically, [12] presented a numerical procedure for the reachability analysis of differential-algebraic equation (DAE) systems. This work computes reachable sets for uncertain initial states and inputs in an over-approximative way and can be used for formal verification of system properties. The work in [5] combines the centralized formal analysis method with quasi-diagonalized Gergorin theory to efficiently assess the stability of networked microgrids and further identify their stability boundaries. Since [5] and [12] are centralized methods, they could be computationally too expensive for evaluating large-scale or configurable power systems.

Distributed formal analysis (or compositional formal analysis) is presented in [7], [13]. As mentioned in [13], two compositional techniques are available. One is to compositionally compute the set of linearization errors, while abstracting the dynamics to linear differential inclusions using the full model as shown in [13]. The other is to split a large-scale interconnected grid into subsystems for which the reachable sets are computed separately as presented in [7].

Formal analysis is a powerful tool beyond existing methods to tackle the stability issues considering inherent parametric and/or input uncertainties from various sources in the grid such as DERs. Although such uncertainties may be tackled by using time- or frequency-domain simulation methods, a near-infinite number of scenarios have to be evaluated. Therefore, the time-domain or frequency-domain simulation methods have limited capabilities in handling uncertainties [14], [15]. Even with Monte Carlo simulations, it is still impossible to verify the infinitely many scenarios that can happen in a real system [16]. Direct methods can provide correctness proofs as it can be done using reachability analysis, but they require to find appropriate Lyapunov functions or contraction functions [17], [18], which is again difficult if not impossible for a relatively large system in reality.

Moreover, centralized stability calculation and evaluation may be impractical for dealing with a large-scale system [19], [20] and may pose privacy issues when used to integrate customer-owned DERs or microgrids [21], [22]. Multiple decomposition techniques offer potent ways to tackle this problem. A coherency-based decomposition method was proposed in [23] to decouple slow electromechanical oscillations from fast ones, in order to study the inter-area mode oscillation phenomenon. However, oscillation modes are very similar among DERs or microgrids [24]. A hierarchical spectral clustering methodology was adopted in [25] to reveal the internal connectivity structure of a power transmission system, in order to properly partition a large-scale system. However, it needed to calculate the eigenvalues and eigenvectors of a matrix correlated to the network, which significantly increases the computational burden and highly limits the wide use of this method. A multi-area Thévenin equivalent circuit approach was used in [26], which focuses more on optimally dividing the computation among several processors. A waveform relaxation method was used in [27] for transient stability simulations, where subsystems' information is still shared between them. In summary, none of them can be effectively used in DER-dominated power networks to solve the above-mentioned stability issue.

In order to overcome the limitations of existing techniques, a scalable privacy-preserving distributed formal analysis (DFA) approach using reachable sets is presented to efficiently analyze the stability of interconnected power systems under disturbances with a focus on large-scale networked microgrids. Specifically, small signal stability under different disturbances is investigated. The novelties of the proposed DFA are threefold:

- An N+M decomposition approach is established to decouple a large-scale networked system and enable distributed reachable set calculations in parallel. It is a microgrid-dominant decomposition only with power injection exchanged between microgrids and the power backbone, which cannot be realized via previous techniques. Thus, not only it renders central coordination unnecessary, but also can make full use of distributed computing resources and drastically reduce computational efforts.
- 2) A programmable data exchange mechanism is developed to make the DFA a privacy-preserving approach that exchanges only limited information with neighboring systems, which has not been considered previously. Therefore, it can help guarantee the privacy and security of information among neighboring systems.

3) The DFA enables the plug-and-play of subsystems (e.g., distribution feeders or microgrids), meaning a subsystem can be easily integrated into or disconnected from an existing system. This function enables DFA to evaluate the stability of a configurable power network online, which cannot be realized via previous techniques.

The remainder of this paper is organized as follows. Section II establishes the methodological foundations of DFA. Section III describes partitioning a large-scale system into small active and passive subsystems using an N+M decomposition approach. Section IV discusses data exchange between subsystems and describes how DFA would be implemented. In Section V, tests on an interconnected networked microgrid system verify the feasibility and effectiveness of DFA. Conclusions are drawn in Section VI.

# II. DISTRIBUTED FORMAL ANALYSIS VIA REACHABLE SET CALCULATION

DFA aims to find the bounds of all possible system trajectories under various disturbances. In this work, we use reachability analysis to bound all solutions. Typically, reachable sets are computed for short time intervals  $\tau_k = [t_k, t_{k+1}]$ , where  $t_k$  and  $t_{k+1}$  are time steps.

#### A. Distributed Formal Analysis

Assuming that a large-scale system is decomposed into several small subsystems, the reachable sets of the overall interconnected system can be obtained based on the results from each subsystem as shown in (1) and (2) [7], [13].

$$\mathcal{R}_s^e(t_{k+1}) = \varphi_1 \mathcal{R}_1^e(t_{k+1}) \times \varphi_2 \mathcal{R}_2^e(t_{k+1}) \times \cdots$$
$$\times \varphi_{N+M} \mathcal{R}_{N+M}^e(t_{k+1}) \tag{1}$$

$$\mathcal{R}_{s}^{e}(\tau_{k}) = \varphi_{1}\mathcal{R}_{1}^{e}(\tau_{k}) \times \varphi_{2}\mathcal{R}_{2}^{e}(\tau_{k}) \times \cdots \times \varphi_{N+M}\mathcal{R}_{N+M}^{e}(\tau_{k})$$
(2)

where  $\mathcal{R}^e_s(t_{k+1})$  is the reachable set at time steps,  $\mathcal{R}^e_s(\tau_k)$  is the reachable set during time intervals, both for the overall system, N+M is the number of subsystems (see Section III),  $\times$  is the Cartesian product,  $\mathcal{R}^e_i(t_{k+1})$  is the reachable set of the ith subsystem at time steps,  $\mathcal{R}^e_i(\tau_k)$  is the reachable set of the ith subsystem during time intervals,  $\varphi_i$  is a matrix of ones and zeros, mapping the local states of the ith subsystem to the states of the overall system.

#### B. Formal Analysis in Each Subsystem

Each subsystem is modeled as a set of semi-explicit, index-1, nonlinear DAEs shown in (3) and (4).

$$\dot{\mathbf{x}}_{\mathbf{i}} = \mathbf{f}_{\mathbf{i}}(\mathbf{x}_{\mathbf{i}}, \mathbf{y}_{\mathbf{i}}, \mathbf{p}_{\mathbf{i}}) \tag{3}$$

$$\mathbf{0} = \mathbf{g_i}(\mathbf{x_i}, \mathbf{y_i}, \mathbf{p_i}) \tag{4}$$

where  $\mathbf{x_i} \in \mathbb{R}^{s_i}$  is the state variable vector (e.g., integral variable in DER controllers) in the *i*th subsystem,  $\mathbf{y_i} \in \mathbb{R}^{q_i}$  is the corresponding algebraic variable vector (e.g., bus voltage), and  $\mathbf{p_i} \in \mathbb{R}^{p_i}$  is the corresponding disturbance vector (e.g., PV fluctuations). Note that DERs' power-electronic interfaces are modeled using the dynamic averaging method [28].

For reachability analysis, we linearize each subsystem at each time step, as presented in [13]:

$$\begin{cases} \dot{\mathbf{x}}_{i} = \mathbf{f}_{i}(\mathbf{x}_{i}^{0}, \mathbf{y}_{i}^{0}, \mathbf{p}_{i}^{0}) + \mathbf{f}_{\mathbf{x}_{i}} \Delta \mathbf{x}_{i} + \mathbf{f}_{\mathbf{y}_{i}} \Delta \mathbf{y}_{i} + \mathbf{f}_{\mathbf{p}_{i}} \Delta \mathbf{p}_{i} \\ 0 = \mathbf{g}_{i}(\mathbf{x}_{i}^{0}, \mathbf{y}_{i}^{0}, \mathbf{p}_{i}^{0}) + \mathbf{g}_{\mathbf{x}_{i}} \Delta \mathbf{x}_{i} + \mathbf{g}_{\mathbf{y}_{i}} \Delta \mathbf{y}_{i} + \mathbf{g}_{\mathbf{p}_{i}} \Delta \mathbf{p}_{i} \end{cases}$$
(5)

where  $(\mathbf{x}_i^0, \mathbf{y}_i^0, \mathbf{p}_i^0)$  is the operation point,  $\mathbf{f}_{\mathbf{x}_i}$ ,  $\mathbf{f}_{\mathbf{y}_i}$ ,  $\mathbf{f}_{\mathbf{p}_i}$ ,  $\mathbf{g}_{\mathbf{x}_i}$ ,  $\mathbf{g}_{\mathbf{y}_i}$ , and  $\mathbf{g}_{\mathbf{p}_i}$  are the partial derivative matrices with respect to variables, given as follows:

$$\begin{split} \mathbf{f}_{\mathbf{x}_i} &= \frac{\partial \mathbf{f_i}}{\partial \mathbf{x_i}} \qquad \mathbf{f}_{\mathbf{y}_i} &= \frac{\partial \mathbf{f_i}}{\partial \mathbf{y_i}} \qquad \mathbf{f}_{\mathbf{p}_i} &= \frac{\partial \mathbf{f_i}}{\partial \mathbf{p_i}} \\ \mathbf{g}_{\mathbf{x}_i} &= \frac{\partial \mathbf{g_i}}{\partial \mathbf{x_i}} \qquad \mathbf{g}_{\mathbf{y}_i} &= \frac{\partial \mathbf{g_i}}{\partial \mathbf{v_i}} \qquad \mathbf{g}_{\mathbf{p}_i} &= \frac{\partial \mathbf{g_i}}{\partial \mathbf{p_i}} \end{split}$$

Since  $\mathbf{g}_{y_i}^{-1}$  always exists for a index-1 DAE system [12], the following equation can be obtained [13].

$$\Delta \dot{\mathbf{x}}_{\mathbf{i}} = [\mathbf{f}_{\mathbf{x}_{\mathbf{i}}} - \mathbf{f}_{\mathbf{y}_{\mathbf{i}}} \mathbf{g}_{\mathbf{y}_{\mathbf{i}}}^{-1} \mathbf{g}_{\mathbf{x}_{\mathbf{i}}}] \Delta \mathbf{x}_{\mathbf{i}} + [\mathbf{f}_{\mathbf{p}_{\mathbf{i}}} - \mathbf{f}_{\mathbf{y}_{\mathbf{i}}} \mathbf{g}_{\mathbf{y}_{\mathbf{i}}}^{-1} \mathbf{g}_{\mathbf{p}_{\mathbf{i}}}] \Delta \mathbf{p}_{\mathbf{i}}$$
(6)

Then each subsystem under uncertainties can be abstracted by the following differential inclusion. Details of the abstraction can be found in [13].

$$\Delta \dot{\mathbf{x}}_{\mathbf{i}} \in \mathbf{A}_{\mathbf{i}} \Delta \mathbf{x}_{\mathbf{i}} \oplus \mathbf{P}_{\mathbf{i}} \tag{7}$$

where  $\mathbf{A_i} = \mathbf{f_{x_i}} - \mathbf{f_{y_i}} \mathbf{g_{y_i}^{-1}} \mathbf{g_{x_i}} = [a_{jk}] \in \mathbb{R}^{q_i \times q_i}$  is the state matrix of the ith subsystem,  $\oplus$  is the Minkowski addition  $(A \oplus B = \{a+b|a \in A, b \in B\})$ , and  $\mathbf{P_i} = [\mathbf{f_{p_i}} - \mathbf{f_{y_i}} \mathbf{g_{y_i}^{-1}} \mathbf{g_{p_i}}] \Delta \mathbf{p_i}$  is a set of uncertain inputs which can be either formulated using a crisp-value-based approach [29] or a set-based one [30].

The reachable set of each subsystem can be over-approximated at each time step via a closed-form solution [13]:

$$\mathcal{R}_{i}^{e}(t_{k+1}) = e^{\mathbf{A}_{i}r} \mathcal{R}_{i}^{e}(t_{k}) \oplus \Psi(\mathbf{A}_{i}, r, \mathbf{p}_{i,0}) \oplus I_{p}^{e}(\mathbf{p}_{i,\Delta}, r) \quad (8)$$

$$\mathcal{R}_{i}^{e}(\tau_{k}) = C(\mathcal{R}_{i}^{e}(t_{k}), e^{\mathbf{A}_{i}r} \mathcal{R}_{i}^{e}(t_{k}) \oplus \Psi(\mathbf{A}_{i}, r, \mathbf{p}_{i,0}))$$

$$\oplus I_{p}^{e}(\mathbf{p}_{i,\Delta}, r) \oplus I_{\varepsilon}^{e} \quad (9)$$

where  $r=t_{k+1}-t_k$  is the time interval,  $C(\cdot)$  returns a convex hull, and  $e^{\mathbf{A_i}r}$  is the matrix exponential.  $\Psi(\mathbf{A_i},r,\mathbf{p_{i,0}})$  and  $I_p^e(\mathbf{p_{i,\Delta}},r)$  represent the additional reachable set caused by deterministic inputs  $\mathbf{p_{i,0}}$  and uncertain ones  $\mathbf{p_{i,\Delta}}$ , as derived in (10) and (11), respectively.  $I_\xi^e$  represents the additional reachable set to consider the curvature of trajectories from  $t_k$  to  $t_{k+1}$ .

$$\Psi(\mathbf{A_{i}}, r, \mathbf{p_{i,0}}) = \left\{ \sum_{j=0}^{\eta} \frac{\mathbf{A_{i}}^{j} r^{j+1}}{(j+1)!} \right.$$

$$\oplus \left[ -X(\mathbf{A_{i}}, r)r, X(\mathbf{A_{i}}, r)r \right] \right\} \mathbf{p_{i,0}} \quad (10)$$

$$I_{p}^{e}(\mathbf{p_{i,\Delta}}, r) = \sum_{j=0}^{\eta} \left( \frac{\mathbf{A_{i}}^{j} r^{j+1}}{(j+1)!} \mathbf{p_{i,\Delta}} \right)$$

$$\oplus \left\{ \left[ -X(\mathbf{A_{i}}, r)r, X(\mathbf{A_{i}}, r)r \right] \otimes \mathbf{p_{i,\Delta}} \right\}$$

$$I_{\xi}^{e} = \left\{ \left( I \oplus [-X(\mathbf{A}_{i}, r), X(\mathbf{A}_{i}, r)] \right) \otimes \mathcal{R}_{i}^{e}(t_{k}) \right\}$$

$$\oplus \left\{ \left( \tilde{I} \oplus [-X(\mathbf{A}_{i}, r)r, X(\mathbf{A}_{i}, r)r] \right) \otimes \mathbf{p}_{i,0} \right\}$$
(12)

where  $\otimes$  is a set-based multiplication  $(A \otimes B = \{ab | a \in A, b \in B\})$ .  $X(\mathbf{A_i}, r), I, \tilde{I}$  involved in (10)–(12) are given in (13)–(15):

$$X(\mathbf{A_i}, r) = e^{|\mathbf{A_i}|r} - \sum_{i=0}^{\eta} \frac{(|\mathbf{A_i}|r)^j}{j!}$$
(13)

$$I = \sum_{j=2}^{\eta} \left[ \left( j^{\frac{-j}{j-1}} - j^{\frac{-1}{j-1}} \right) r^j, 0 \right] \frac{\mathbf{A_i}^j}{j!}$$
 (14)

$$\tilde{I} = \sum_{j=2}^{\eta+1} \left[ \left( j^{\frac{-j}{j-1}} - j^{\frac{-1}{j-1}} \right) r^j, 0 \right] \frac{\mathbf{A_i}^{j-1}}{j!}$$
 (15)

More detailed derivations of the above expressions can be found in [5], [12].

## III. PARTITIONING LARGE-SCALE POWER NETWORKS WITH DERS

It can be computationally expensive to directly implement formal analysis on a large-scale networked system. Therefore, grid decomposition offers a solution for scalable DFA.

#### A. N + M Decomposition

In this section, an N+M decomposition method is presented to partition a large-scale power network into several smaller subsystems. Subsystems are coupled by power injection [31], [32], as shown in Fig. 1(a).

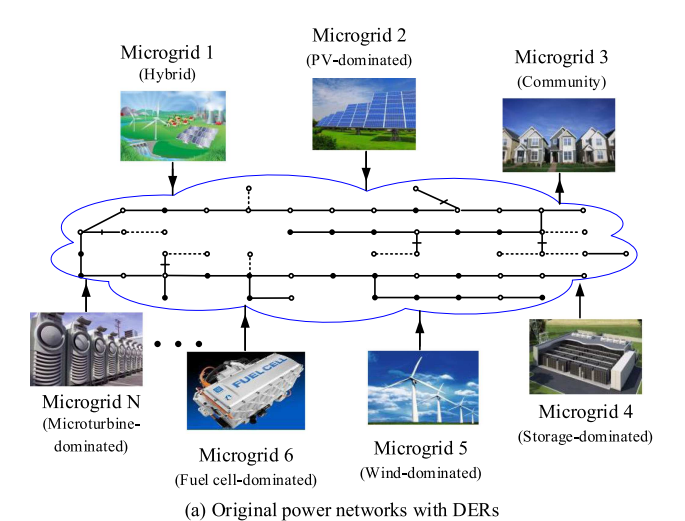
Based on whether a subsystem integrates DERs, the original large-scale power network can be divided into N+M subsystems, as shown in Fig. 1(b), where N is the number of active subsystems (i.e., energized by DERs), and M is the number of passive subsystems (i.e., power backbone).

Then by using the N+M decomposition technique, the power flow equation of an overall power network can be rewritten as follows:

$$\mathbf{Y}_{\mathrm{ext}} \cdot \mathbf{V}_{\mathrm{ext}} \circ \overline{\mathbf{V}}_{\mathrm{ext}} + \mathbf{S}_{\mathrm{ext}}^{\mathrm{G}} - \mathbf{S}_{\mathrm{ext}}^{\mathrm{L}} - \mathbf{S}_{\mathrm{ext}}^{\mathrm{I}} = \mathbf{0}$$
 (16)

where  $\circ$  is the Hadamard product  $((A \circ B)_{ij} = [a_{ij} \cdot b_{ij}], a_{ij} \in A, b_{ij} \in B)$ . The other variables in (16) are introduced as follows:

1) Extended Admittance Matrix: In (16),  $\mathbf{Y_{ext}}$  is the extended admittance matrix under system partitions as shown in (17), where  $\mathbf{Y}_{11}, \ldots, \mathbf{Y}_{NN}$  are the extended admittance matrices correlated to the active subsystems, and  $\mathbf{Y}_{N+1,N+1}, \ldots, \mathbf{Y}_{N+M,N+M}$  are the extended admittance matrices correlated to the passive subsystems. The entries of  $\mathbf{Y}_{ii}$ 



Subsystem 1

Subsystem 1

Subsystem •

Active Subsystems

Active Subsystems

Fig. 1. Concept of power network partition using N + M decomposition.

(b) Decoupled subsystems

are shown in (18).

 $Y_{ext} =$ 

$$Y_{ii} = \begin{bmatrix} Y_{11} & \cdots & \mathbf{0} & \mathbf{0} & \cdots & \mathbf{0} \\ \vdots & \ddots & \vdots & \vdots & \ddots & \vdots \\ \mathbf{0} & \cdots & Y_{NN} & \mathbf{0} & \cdots & \mathbf{0} \\ \mathbf{0} & \cdots & \mathbf{0} & Y_{N+1,N+1} & \cdots & \mathbf{0} \\ \vdots & \ddots & \vdots & \vdots & \ddots & \vdots \\ \mathbf{0} & \cdots & \mathbf{0} & \mathbf{0} & \cdots & Y_{N+M,N+M} \end{bmatrix}$$

$$Y_{ii} = \begin{bmatrix} |y_{11}|\cos\beta_{11} & |y_{12}|\cos\beta_{12} & \cdots & |y_{1k}|\cos\beta_{1k} \\ |y_{21}|\cos\beta_{21} & |y_{22}|\cos\beta_{22} & \cdots & |y_{2k}|\cos\beta_{2k} \\ \vdots & \vdots & \ddots & \vdots \\ |y_{k1}|\cos\beta_{k1} & |y_{k2}|\cos\beta_{k2} & \cdots & |y_{kk}|\cos\beta_{kk} \\ |y_{11}|\sin\beta_{11} & |y_{12}|\sin\beta_{12} & \cdots & |y_{1k}|\sin\beta_{1k} \\ |y_{21}|\sin\beta_{21} & |y_{22}|\sin\beta_{22} & \cdots & |y_{2k}|\sin\beta_{2k} \\ \vdots & \vdots & \ddots & \vdots \\ |y_{k1}|\sin\beta_{k1} & |y_{k2}|\sin\beta_{k2} & \cdots & |y_{kk}|\sin\beta_{kk} \end{bmatrix}$$

$$(18)$$

where the admittance between the node l and node k is expressed as  $y_{lk} = |y_{lk}| \cos \alpha_{lk} + j|y_{lk}| \sin \alpha_{lk}, |y_{lk}|$  is the absolute value of the branch admittance,  $\alpha_{lk}$  is the corresponding angle of the branch admittance,  $\beta_{lk} = \theta_l - \theta_k - \alpha_{lk}$ , and  $\theta_l, \theta_k$  are the voltage angles at the node l and node k, respectively.

2) Extended Voltage Vectors: In (16),  $V_{\rm ext}$  is the bus voltage vector after system partition as shown in (19),  $\overline{V}_{\rm ext}$  is the extended bus voltage vector as shown in (20).

$$\mathbf{V_{ext}} = \begin{bmatrix} \mathbf{V_{11}}, & \dots, & \mathbf{V_{NN}}, & \dots, & \mathbf{V_{N+M,N+M}} \end{bmatrix}^{T}$$
(19)
$$\overline{\mathbf{V}_{ext}} = \begin{bmatrix} \mathbf{V_{11}}, & \mathbf{V_{11}}, & \dots, \mathbf{V_{NN}}, \\ \mathbf{V_{NN}}, & \dots, & \mathbf{V_{N+M,N+M}}, & \mathbf{V_{N+M,N+M}} \end{bmatrix}^{T}$$
(20)

where  $V_{11}, \ldots, V_{NN}$  are the voltage vectors in the active subsystems, and  $V_{N+1,N+1}, \ldots, V_{N+M,N+M}$  are the voltage vectors in the passive subsystems.

- 3) Extended Power Vectors: In(16),  $\mathbf{S_{ext}^G}$  is the vector showing power injections from DERs to active subsystems;  $\mathbf{S_{ext}^L}$  is the vector of power loads in each subsystem; and  $\mathbf{S_{ext}^I}$  is the vector of exchange power on the interfaces between subsystems and has the following properties:
  - When line loss is considered during calculation, S<sup>1</sup><sub>ext,i</sub> and S<sup>I'</sup><sub>ext,i</sub> in Fig. 1(b) are different; otherwise, they are the same.
  - Some of the entries in S<sup>I</sup><sub>ext</sub> are correlated with others, which means they need to be updated together at each time step. This issue is solved by the proposed status flag method introduced in Section IV.

#### B. Partitioning Large-Scale Power Networks

Because DERs are not supposed to appear in passive susbsystems under the N+M decomposition, the entries in  $\mathbf{S_{ext}^G}$ correlated to the passive subsystems is zero. Then, the algebraic equations of the overall system can be rewritten as follows:

$$\begin{cases} \mathbf{Y}_{kk} \cdot \mathbf{V}_{kk} \circ \overline{\mathbf{V}}_{kk} + \mathbf{S}_{kk}^G - \mathbf{S}_{kk}^L - \mathbf{S}_{kk}^I = 0 \\ \mathbf{Y}_{jj} \cdot \mathbf{V}_{jj} \circ \overline{\mathbf{V}}_{jj} - \mathbf{S}_{jj}^L - \mathbf{S}_{jj}^I = 0 \end{cases} \tag{21}$$

where k = 1, ..., N, j = N + 1, ..., N + M.

From (21), it can be seen that the admittance matrix of the original entire system is fully decoupled into several independent sub-matrices, because of the introduction of equivalent power injections on the interfaces between subsystems. Therefore, the calculation of  $\mathbf{S}_{\text{ext}}^{\mathbf{I}}$  is essential and is introduced in Section IV.

#### IV. IMPLEMENTATION OF DFA IN POWER NETWORKS

#### A. Procedure of DFA

Our overall procedure for DFA is presented in Fig. 2. Initially, the N+M decomposition is used to partition an interconnected power network into several subsystems modeled as in (3) and (4). The set of power flow in each subsystem is calculated in parallel based on data exchange between subsystems.

Next, subsystems' linearization is conducted via (5). In a next step, (8) and (9) are used to compute reachable sets in each

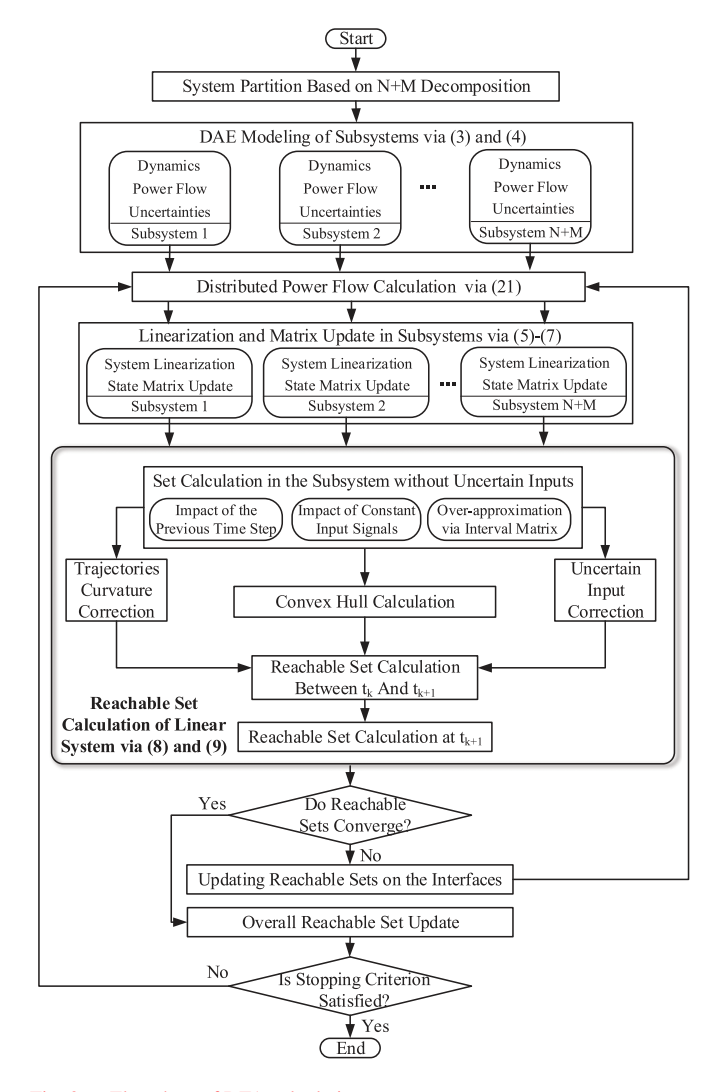


Fig. 2. Flowchart of DFA calculation.

subsystem in parallel based on reachable sets exchange between subsystems. If the reachable sets on the interfaces converge, the overall reachable set can be obtained based on (1) and (2). Otherwise, the power flow is updated and reachable sets in each subsystem are re-computed. More details about reachable sets calculation can be found in [13].

The DFA process terminates when the simulation time ends or the reachable set results are too conservative to be useful.

#### B. Distributed Algorithm and Data Exchange

Two nested iterations are used in the distributed algorithm, where the inner loop solves power flow or computes reachable sets in each subsystem while the outer loop updates exchange power until the stopping criterion is met. The overall iteration process is terminated when one of the following two criteria is satisfied:

$$\Delta \mathbf{s_{ki}} \le \epsilon_o$$
 (22)

$$L_o > Iter_o^{\max}$$
 (23)

where  $\Delta s_{ki} = Y_{ki} \cdot V_{ki} \circ \overline{V}_{ki} - Y_{ki} \cdot V_{ki}^P \circ \overline{V}_{ki}^P$  is the change of power exchange between subsystem k and subsys-

tem i,  $\mathbf{V_{ki}} = [\mathbf{V_k}, \mathbf{V_i}]$  is the voltage vector at the current step,  $\mathbf{V_{ki}^P} = [\mathbf{V_k^P}, \mathbf{V_i^P}]$  is the voltage vector at the previous step,  $\epsilon_o$  is a given threshold of the outer loop iteration,  $L_o$  is the iteration number, and  $Iter_o^{\max}$  is the given upper limit of iteration number.

1) Distributed Algorithm: The power transferred through coupling lines is exchanged among two neighboring subsystems, i.e.,  $\mathbf{S}_{\text{ext}}^{\mathbf{I}}$  shown in Fig. 1(b) and  $\mathbf{S}_{\mathbf{k}\mathbf{k}}^{\mathbf{I}}$  or  $\mathbf{S}_{\mathbf{j}\mathbf{j}}^{\mathbf{I}}$  in (21). Specifically, they are updated based on the interface voltage of their neighboring subsystems, as shown in (24), where the power flow calculation in the passive subsystem j is given as an example:

$$\begin{cases} \mathbf{Y}_{jj} \cdot \mathbf{V}_{jj} \circ \overline{\mathbf{V}}_{jj} - \mathbf{S}_{jj}^{\mathbf{L}} - \mathbf{S}_{jj}^{\mathbf{I}} = \mathbf{0} \\ \mathbf{S}_{jj}^{\mathbf{I}} = \mathbf{Y}_{ji} \cdot \mathbf{V}_{ji} \circ \overline{\mathbf{V}}_{ji} \end{cases}$$
(24)

where  $\mathbf{Y_{ji}}$  is the admittance matrix of the interface branch between subsystem j and its neighboring subsystem i, the expression of  $\mathbf{Y_{ji}}$  can be derived via (18),  $\mathbf{V_{ji}} = [\mathbf{V_{j}}, \mathbf{V_{i}^{P}}]$  is the voltage vector. Once the interface voltage  $\mathbf{V_{i}^{P}}$  is obtained from previous iterations in subsystem i, it will be treated as a reference bus and maintain a constant value until the computation of power flow (or reachable sets) in subsystem j completes, i.e.,  $\mathbf{V_{j}}$  is obtained. The aforementioned inner loop iteration is terminated when one of the following two criteria is satisfied:

$$\Delta \mathbf{V_{jj}} \le \epsilon_i$$
 (25)

$$L_i > Iter_i^{\max}$$
 (26)

where  $\Delta V_{jj}$  is the voltage increments between iterations in subsystem j,  $\epsilon_i$  is a given threshold of the inner loop iteration,  $L_i$  is the iteration number, and  $Iter_i^{\max}$  is the given upper limit of iteration number.

Note that, during the inner loop iterations in subsystem j, the power exchange between subsystem j and subsystem i is updated correspondingly at each iteration step due to the update of  $\mathbf{V_j}$  in subsystem j. Thus, physical laws (e.g., Ohms law) on the line linking two subsystems are fully respected for each time interval

2) Data Exchange Between Subsystems: Since both power flow calculation and reachable set computation in subsystems are carried out based on interface information, data exchange between subsystems plays an essential role in our DFA implementation. Taking into account different iterations and calculation times which may be used in subsystems, we introduce a status *flag* to communicate the computation progress in each subsystem, as defined in (27):

$$Flag = [Subsystem-ID, Convergence, Results]$$
 (27)

where *Subsystem-ID* is the ID of the neighboring subsystem, *Convergence* is a binary indicator of whether the subsystem is converged or not, where 1 means convergence and 0 means not converged, *Results* are the final voltages at the interface after the iteration in this subsystem stops. The use of *flag* is inspired by [33]; its update can be implemented, for instance, through a software-defined technique as detailed in [34].

The introduction of the status Flag concept has the following three advantages:

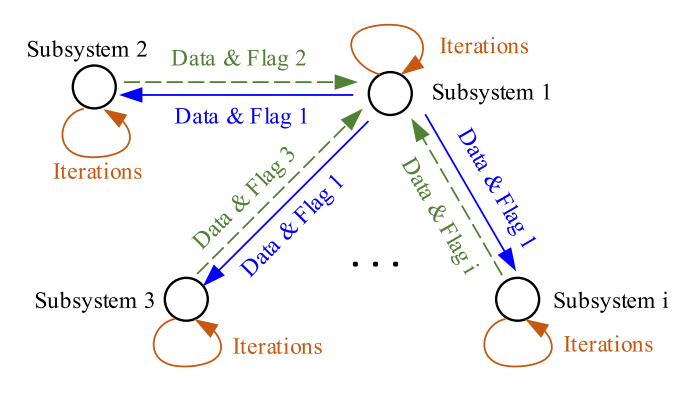


Fig. 3. Data exchange between subsystems.

- Each subsystem always uses the latest converged results from its neighboring subsystems.
- It is a privacy-preserving design with only interface data transferred, which means it helps ensure data security. In the future, we will use a data encryption technique to ensure the integrity and confidentiality of the interface data, and to protect against attacks such as monster-in-the-middle (MitM) attacks.
- Flag is modifiable, which means features can be easily added or removed based on needs.

The basic idea of data exchange is given in Fig. 3, with the following three steps involved within one time step:

- 1) Each subsystem updates the information of its interface with other subsystems, i.e.,  $\mathbf{S}_{kk}^{\mathbf{I}}$  or  $\mathbf{S}_{jj}^{\mathbf{I}}$  in (21). Specifically, in distributed power flow calculation, they are crisp-value-based data, whereas in subsystems' reachable set calculation, it is set-based data. Meanwhile, status Flags are transmitted as well to confirm the validity of the data.
- 2) Once status Flags correlated to one subsystem show all its interface data is available, the inner loop power flow or reachable set calculation will be carried out. For example, subsystem 1 will not run its calculation until it receives the interface data and status Flags from subsystems 2, 3, and i, when they are interconnected as shown in Fig. 3. Therefore, power flows or reachable sets will be computed in parallel based on the data from last iterations in the neighboring subsystem.
- 3) After the iterations in the subsystems finish, the corresponding interface data and status Flags are broadcast to their neighbors in the outer loop for the next iteration.

#### V. TEST AND VALIDATION OF DFA

A typical networked microgrid system shown in Fig. 4 is used to test and validate the presented DFA approach by analyzing what impact is imposed by DERs on system dynamics. In order to better illustrate this impact, the networked microgrid system is operated in islanded mode, which means the circuit breaker is open. More details of the test system can be found in [5]. The DFA algorithms are developed on the basis of the CORA toolbox [35]. The simulation step size is set to 0.01 s.

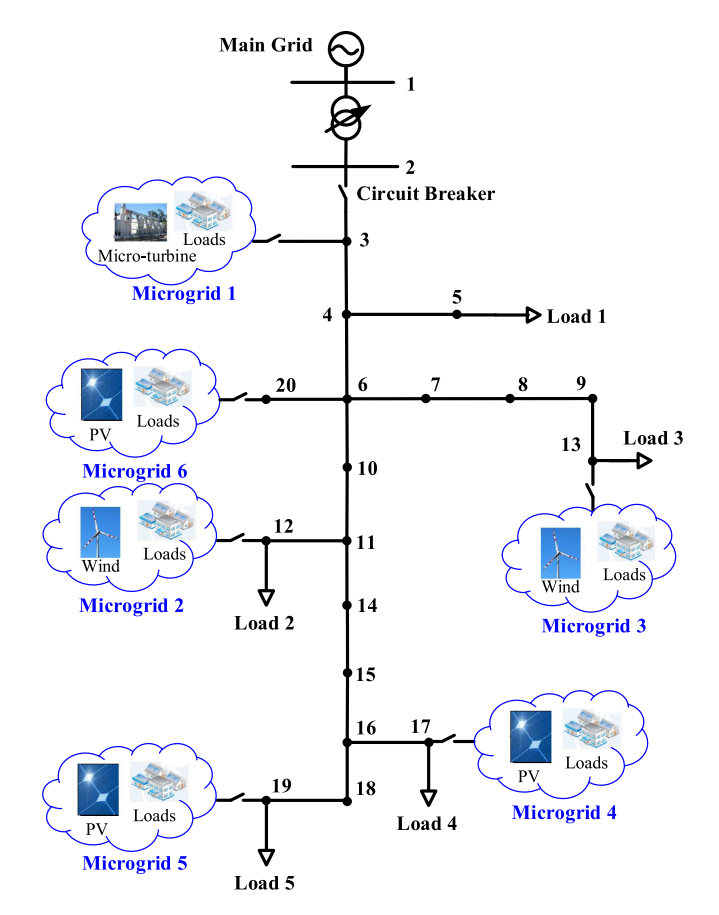


Fig. 4. A typical networked microgrid system.

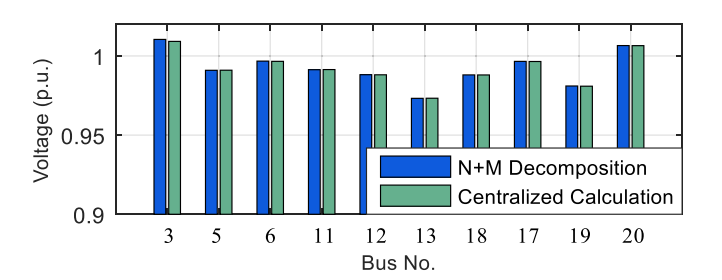


Fig. 5. Voltage magnitude comparison in Case I.

#### A. Verification of N + M Decomposition

In order to better validate the effectiveness of the N+M decomposition, two different partitions are presented.

1) Case I. Partitioning Into Two Subsystems: The original networked microgrid system is partitioned into two active subsystems: N=2 and M=0 in (21). Specifically, the branch between node 6 and node 10 is broken down, i.e., subsystem 1 comprises microgrids 1, 3, and 6, whereas subsystem 2 comprises microgrids 2, 4, and 5. Based on the partitioning described above, subsystem 1 conducts its power flow calculation by using the power injection from node 10. At the same time, subsystem 2 conducts power flow calculation by using the power injection from node 6.

Fig. 5 shows the voltage magnitude comparison between the N+M decomposition method and the centralized calculation.

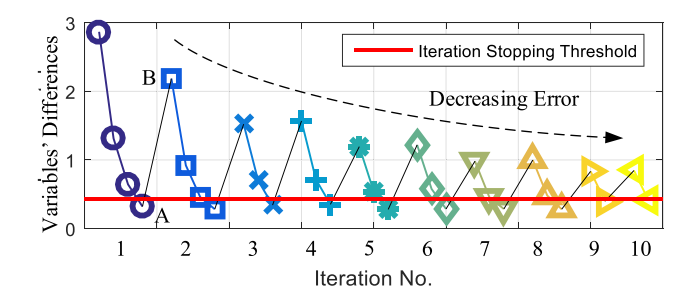


Fig. 6. Iterations of power flow calculation in the subsystem 1 in Case I.

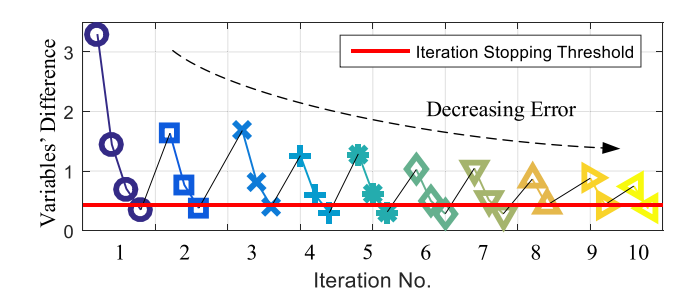


Fig. 7. Iterations of power flow calculation in the subsystem 2 in Case I.

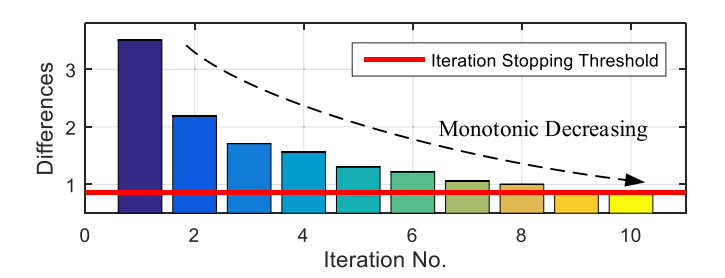


Fig. 8. Iterations on the interface of two subsystems.

Fig. 6 and Fig. 7 show the changes of variables during the Newton iterations in subsystem 1 and subsystem 2, respectively. Fig. 8 demonstrates the differences of power injections on the interface between the current iteration and the previous one. The stopping criteria of subsystem 1 and subsystem 2 are set as  $\epsilon_i = 1.0e - 10$ , whereas that of their interface is set as  $\epsilon_o = 1.0e - 5$ . In order to better illustrate the value changes during iterations, the L2 expression is adopted with the following conversion [36]:

$$||r_i||_2 = -10/ln(||v_i||_2)$$
 (28)

where  $||r_i||_2$  is the L2 value shown in figures at each point, and  $||v_i||_2$  is the corresponding L2 value of the real value during iterations.

From Figs. 5–8, it can be seen that:

- Result comparisons on Fig. 5 have verified the feasibility and effectiveness of N + M decomposition in distributed power flow calculation.
- The calculation in each subsystem is a non-monotonic process. The reason is that calculations in each subsystem are carried out based on the interface data ( $\mathbf{S}_{\mathbf{k}\mathbf{k}}^{\mathbf{I}}$  and  $\mathbf{S}_{\mathbf{j}\mathbf{j}}^{\mathbf{I}}$  in (21)) at the previous iteration step. However, after subsystems exchange data, their incrementals involved in the Newton iteration may become large again at the next iteration step

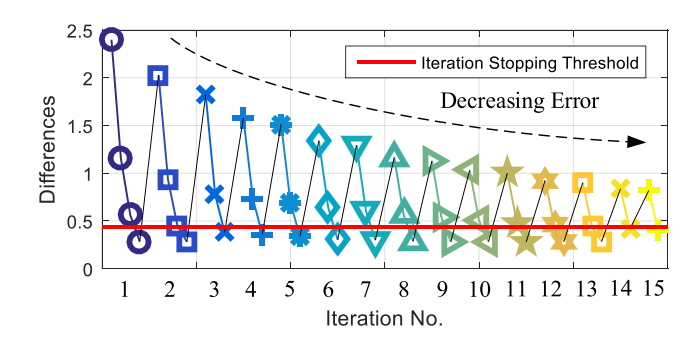


Fig. 9. Iterations of power flow calculation in the subsystem 1 in Case II.

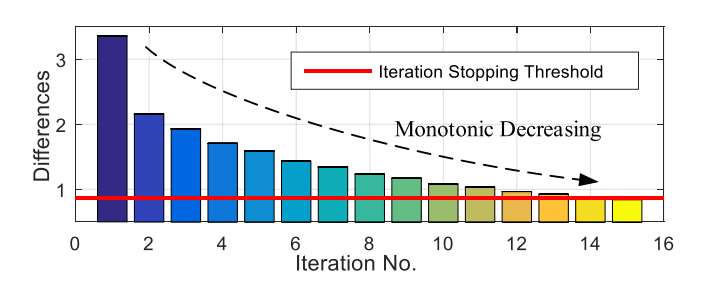


Fig. 10. Iterations on the interface in Case II

(e.g., point B in Fig. 6) even though the current step is converged (e.g., point A in Fig. 6).

- Sub-iterations in subsystems may be different from each other, which validates the necessity of status Flags. For example, during iteration step 2, four sub-iterations are needed before the calculation is converged in subsystem 1; however, only three sub-iterations are involved in subsystem 2.
- The iterations on the interface of subsystems are monotonically decreasing, which means N+M decomposition is an effective method in distributedly calculating the power flow of networked microgrids.
- 2) Case II. Partitioning Into Four Subsystems: In this test, the original networked microgrid system is decoupled into four subsystems to further validate the N+M decomposition and compare it with the results in case I. Specifically, the broken branches are 6-7, 6-10, 15-16. The other settings are the same as those in case I. Fig. 9 shows the changes of variables during iterations in subsystem 1 which includes microgrid 1 and microgrid 6. Fig. 10 demonstrates the differences in power injection on the interface between the current iteration and the previous one.

We gain the following insights from comparing case I with II:

- The more subsystems there are, the less calculation time it may need to finish one iteration in each subsystem. For instance, in Fig. 6, 0.05 s is taken to complete the four subiterations in the first iteration. Meanwhile, it only takes 0.03 s to finish the four iterations in case II, which is only 60% of that in case I.
- From Figs. 6–10, it can be seen that the more subsystems there are, the more iterations it may need to converge. For instance, it takes 10 iterations to finally converge in case I, whereas it requires 15 iterations in case II. This

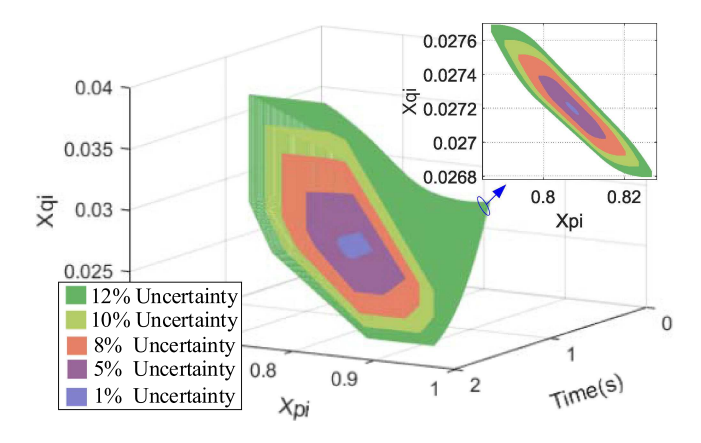


Fig. 11. 3-D reachable sets of  $X_{pi}$ ,  $X_{qi}$  in Microgrid 3 of the subsystem 1.

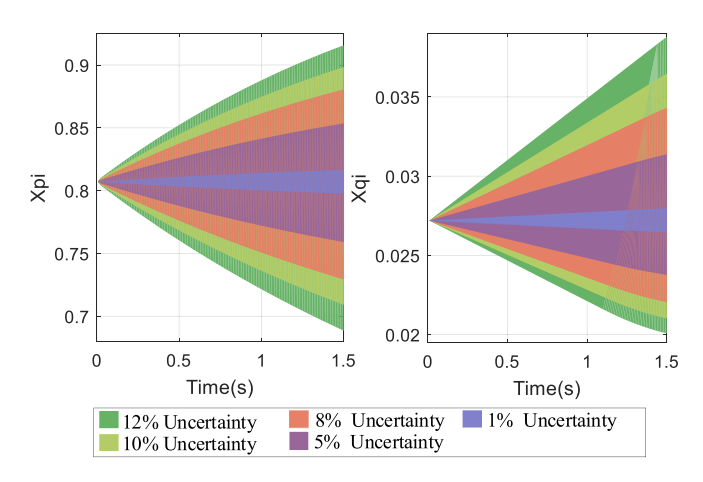


Fig. 12. Reachable sets of  $X_{pi}\,,X_{qi}$  in Microgrid 3 of the subsystem 1 projected to the time line.

intuitive result is caused by the frequent data exchange between subsystems.

## B. Reachable Set Calculation via DFA

In this test, case I is adopted. Meanwhile, multiple active power fluctuations are introduced in microgrid 2, i.e.,  $\pm 1\%, \pm 5\%, \pm 8\%, \pm 10\%$  and  $\pm 12\%$  around its baseline power output.

1) Reachability Analysis: Fig. 11 shows the three dimensional reachable set along the time line with a cross section zoomed in at 0.2 s, where x-axis shows simulation time, y-axis shows the value of control variable of active power  $(X_{pi})$ , z-axis shows the value of control variable of reactive power  $(X_{qi})$ . Fig. 12 and Fig. 13 show the cross sectional views of reachable sets in microgrid 3 and microgrid 4, respectively. More details of  $X_{pi}$  and  $X_{qi}$  can be found in [5].

From Figs. 11–13, it can be seen that:

• DFA is able to calculate the operation boundaries of a networked microgrid system subject to different uncertainty levels, which validates that the presented N+M decomposition technique can be effectively combined with the reachability analysis.

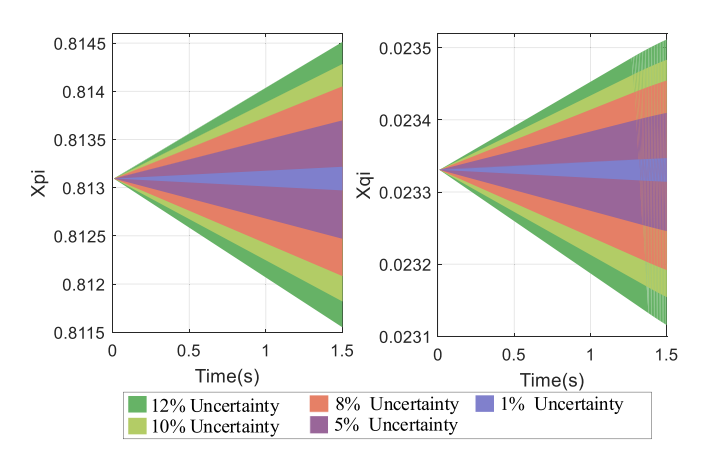


Fig. 13. Reachable sets of  $X_{pi}, X_{qi}$  in Microgrid 4 of the subsystem 2 projected to the time line.

TABLE I
DEVIATIONS COMPARISON BETWEEN ACTIVE AND REACTIVE POWER

Uncertainties	Deviations of Active Power	Deviations of Reactive Power
±1%	[-1.17%, 1.16%]	[-2.73%, 2.84%]
$\pm 5\%$	[-5.96%, 5.74%]	[-12.57%, 15.39%]
$\pm 8\%$	[-9.64%, 9.09%]	[-18.93%, 26.18%]
$\pm 10\%$	[-12.15%, 11.29%]	[-22.72%, 34.09%]
±12%	[-14.70%, 13.45%]	[-26.18%, 42.65%]

- The zoomed-in plot in Fig. 11 shows that the size of reachable sets increase as the uncertainty level increases. The correctness of the DFA result is further verified by the comparison between DFA and the centralized formal analysis via reachable set (FAR) as shown in [5], which is not shown here due to the exact same results.
- Fluctuations in active power can also impact microgrids' reactive power output as shown in Fig. 12 and Fig. 13 due to the presence of resistances in backbone feeders [28]. For instance, Table I summarizes the deviations of  $X_{pi}$  and  $X_{qi}$  at 1.5 s based on the results shown in Fig. 12.
- Since reachable sets enclose the bound of all system trajectories, different disturbances may lead to different reachable sets; and thus, it can be used to pinpoint critical disturbances on stability. Furthermore, it can be adopted to estimate the stability margin of power systems subject to uncertainties [5].
- 2) Impacts of DERs on Interconnected Systems: To better illustrate how stability issues deteriorate and what impact is imposed by DERs on the interconnected grid, more severe DER disturbances are introduced in microgrid 2, i.e.,  $\pm 20\%$  and  $\pm 30\%$  around its baseline active power output at 0.5 s and 1.0 s, respectively. Fig. 14 shows the cross sectional views of reachable sets in microgrid 3, from which it can be seen that:
  - When more severe disturbances are considered in DERs, the size of cross-section of the reachable sets (possible values of all system trajectories at a given point in time) drastically increase or even system trajectories may diverge quickly from its original operation point as shown in Fig. 14. This is consistent with the engineering experience, that the stability of the interconnected system deteriorates

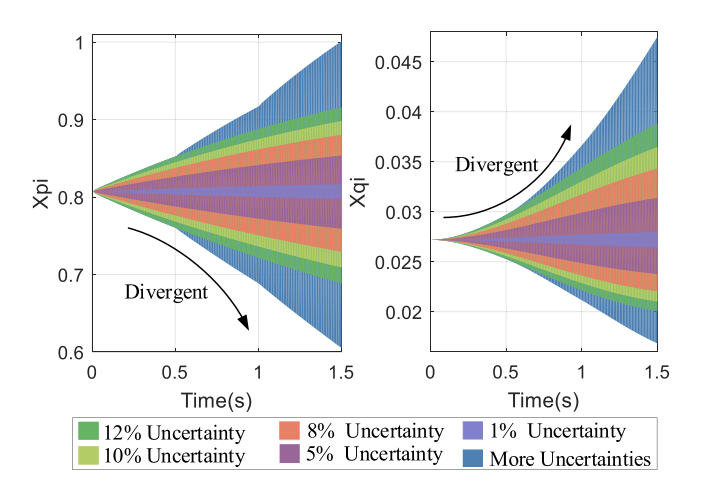


Fig. 14. Reachable sets of  $X_{p\,i}, X_{q\,i}$  in Microgrid 3 when more uncertainties are introduced.

TABLE II
CALCULATION TIMES FOR 1.5 S DYNAMICS ON A 3.4 GHZ PC

Uncertainties	±1%	±5%	±8%	±10%	$\pm 12\%$
DFA (s)	7.5389	7.7167	7.7741	7.8023	8.4692
FAR (s)	6.2591	7.5983	7.6089	7.6149	7.9167
TDS (s)	6.3284	6.3165	6.4726	6.4237	6.4827

with the integration of more DERs without a proper coordination.

 Through reachable set results, critical disturbances can be pinpointed, and further actions (e.g., adaptive control) can be conducted to enhance the stability of interconnected systems.

Besides, the results in [13] also show how the stability performance deteriorates when distributed generations are integrated into systems.

3) Efficiency of DFA: The computation times among DFA, FAR, and time domain simulations (TDS) are given in Table II, where ten calculations of TDS has been considered for comparison.

From Table II, it can be seen that:

- DFA is a competitive and efficient method in calculating reachable sets and analyzing stability performance.
- The results from one run of DFA calculation are able to enclose all possible (infinitely many) system trajectories obtained via TDS, which means DFA is always more efficient than deterministic TDS.
- DFA takes a little more calculation time than FAR due to data exchange between subsystems.
- Because the complexity of reachability analysis is  $O(n^5)$  [13], DFA will outperform FAR or TDS when the system scale n is large enough. It also justifies the potential and efficiency of DFA in handing large-scale power systems.
- 4) Reachable Set Changes During Iterations: Fig. 15 shows the iteration process of the reachable set between  $X_{pi}$  and  $X_{qi}$  in microgrid 3 at 0.2 s and 1.0 s, respectively. From Fig. 15, it can be seen that:

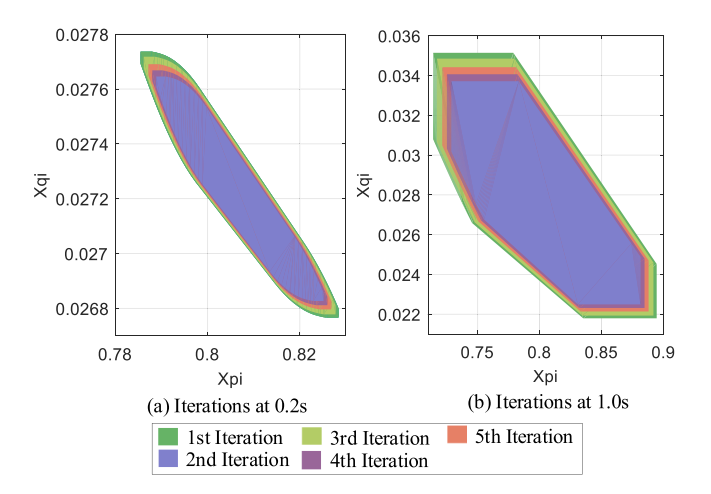


Fig. 15. Reachable set iterations.

- Converged reachable sets in subsystems can be obtained after several iterations.
- Reachable sets can be calculated via parallel iterations, which enables the plug and play of subsystems and makes the corresponding distributed stability analysis possible.

#### VI. CONCLUSIONS

We have presented a novel distributed formal analysis (DFA) enabling efficient stability analysis of large interconnected power grids under a high penetration of DERs. An N+M decomposition method is presented to decouple large-scale systems to compute reachable sets more efficiently while also preserving information privacy within the subsystems. Numerical tests on a typical networked microgrid system have confirmed the feasibility and effectiveness of DFA.

DFA will be applicable for not only forecasting and monitoring grid performance, but also formally verifying various resiliency enhancement strategies such as new schemes for system integrity protection and automation to facilitate the extensive employment of DERs. In our future work, we will further extend DFA to obtain possible operation ranges of microgrid systems. Our quasi-diagonalized Geršgorin method presented in [5] will be upgraded to a distributed version which will be further integrated with DFA to enable more efficient calculation of stability margin.

### REFERENCES

- [1] Z. Bie, P. Zhang, G. Li, B. Hua, M. Meehan, and X. Wang, "Reliability evaluation of active distribution systems including microgrids," *IEEE Trans. Power Syst.*, vol. 27, no. 4, pp. 2342–2350, Nov. 2012.
- [2] Y. Yoldaş, A. Önen, S. Muyeen, A. V. Vasilakos, and İ. Alan, "Enhancing smart grid with microgrids: Challenges and opportunities," *Renewable Sustain. Energy Rev.*, vol. 72, pp. 205–214, 2017.
- [3] Y. Li, P. Zhang, L. Ren, and T. Orekan, "A Geršgorin theory for robust microgrid stability analysis," in *Proc. IEEE Power Energy Soc. Gen. Meeting*, Boston, MA, USA, 2016, pp. 1–5.
- [4] A. Saint-Pierre and P. Mancarella, "Active distribution system management: A dual-horizon scheduling framework for DSO/TSO interface under uncertainty," *IEEE Trans. Smart Grid*, vol. 8, no. 5, pp. 2186–2197, Sep. 2017.
- [5] Y. Li, P. Zhang, and P. B. Luh, "Formal analysis of networked microgrids dynamics," *IEEE Trans. Power Syst.*, vol. 33, no. 3, pp. 3418–3427, May 2018.

- [6] A. El-Guindy, K. Schaab, B. Schürmann, D. Han, O. Stursberg, and M. Althoff, "Formal LPV control for transient stability of power systems," in *Proc. IEEE Power Energy Soc. Gen. Meeting*, Chicago, IL, USA, 2017, pp. 1–5.
- [7] A. El-Guindy, Y. C. Chen, and M. Althoff, "Compositional transient stability analysis of power systems via the computation of reachable sets," in *Proc. Amer. Control Conf.*, 2017, pp. 2536–2543.
- [8] Y. Susuki et al., "A hybrid system approach to the analysis and design of power grid dynamic performance," Proc. IEEE, vol. 100, no. 1, pp. 225– 239, Jan. 2012.
- [9] Y. Susuki, T. Sakiyama, T. Ochi, T. Uemura, and T. Hikihara, "Verifying fault release control of power system via hybrid system reachability," in *Proc. 40th North Amer. Power Symp.*, 2008, pp. 1–6.
- [10] S. Chong et al., "Report on the NSF workshop on formal methods for security," 2016, arXiv:1608.00678.
- [11] X. Jiang, Y. C. Chen, and A. D. Domínguez-García, "A set-theoretic framework to assess the impact of variable generation on the power flow," *IEEE Trans. Power Syst.*, vol. 28, no. 2, pp. 855–867, May 2013.
- [12] M. Althoff and B.-H. Krogh, "Reachability analysis of nonlinear differential-algebraic systems," *IEEE Trans. Autom. Control*, vol. 59, no. 2, pp. 371–383, Feb. 2014.
- [13] M. Althoff, "Formal and compositional analysis of power systems using reachable sets," *IEEE Trans. Power Syst.*, vol. 29, no. 5, pp. 2270–2280, Sep. 2014.
- [14] N. Duan and K. Sun, "Power system simulation using the multistage Adomian decomposition method," *IEEE Trans. Power Syst.*, vol. 32, no. 1, pp. 430–441, Jan. 2017.
- [15] J. Kwon, X. Wang, F. Blaabjerg, and C. L. Bak, "Frequency-domain modeling and simulation of DC power electronic systems using harmonic state space method," *IEEE Trans. Power Electron.*, vol. 32, no. 2, pp. 1044–1055, Feb. 2017.
- [16] T.-E. Huang, Q. Guo, and H. Sun, "A distributed computing platform supporting power system security knowledge discovery based on online simulation," *IEEE Trans. Smart Grid*, vol. 8, no. 3, pp. 1513–1524, May 2017.
- [17] H.-D. Chang, C.-C. Chu, and G. Cauley, "Direct stability analysis of electric power systems using energy functions: Theory, applications, and perspective," *Proc. IEEE*, vol. 83, no. 11, pp. 1497–1529, Nov. 1995.
- [18] H.-D. Chiang, F. F. Wu, and P. P. Varaiya, "A BCU method for direct analysis of power system transient stability," *IEEE Trans. Power Syst.*, vol. 9, no. 3, pp. 1194–1208, Aug. 1994.
- [19] E. Ghahremani and I. Kamwa, "Local and wide-area PMU-based decentralized dynamic state estimation in multi-machine power systems," *IEEE Trans. Power Syst.*, vol. 31, no. 1, pp. 547–562, Jan. 2016.
- [20] Q. Zhou, K. Sun, K. Mohanram, and D. C. Sorensen, "Large power grid analysis using domain decomposition," in *Proc. Des. Automat. Test Eur. Conf.*, 2006, vol. 1, pp. 1–6.
- [21] A. Hussain, V.-H. Bui, and H.-M. Kim, "A resilient and privacy-preserving energy management strategy for networked microgrids," *IEEE Trans. Smart Grid*, vol. 9, no. 3, pp. 2127–2139, May 2018.
- [22] S. A. Salinas and P. Li, "Privacy-preserving energy theft detection in microgrids: A state estimation approach," *IEEE Trans. Power Syst.*, vol. 31, no. 2, pp. 883–894, Mar. 2016.
- [23] J. H. Chow, "Time-scale separation in power system swing dynamics: Singular perturbations and coherency," in *Encyclopedia of Systems and Control*. London, U.K.: Springer, 2015, pp. 1465–1469.
- [24] Y. Li, W. Gao, and J. Jiang, "Stability analysis of microgrids with multiple DER units and variable loads based on MPT," in *Proc. IEEE Power Energy Soc. Gen. Meeting*, National Harbor, MD, USA, 2014, pp. 1–5.
- [25] R. J. Sánchez-García et al., "Hierarchical spectral clustering of power grids," IEEE Trans. Power Syst., vol. 29, no. 5, pp. 2229–2237, Sep. 2014.
- [26] P. Zhang, J. Marti, and H. Dommel, "Network partitioning for real-time power system simulation," in *Proc. Int. Conf. Power Syst. Transients*, Montreal, QC, Canada, 2005, pp. 1–6.
- [27] M. Crow and M. Ilic, "The parallel implementation of the waveform relaxation method for transient stability simulations," *IEEE Trans. Power Syst.*, vol. 5, no. 3, pp. 922–932, Aug. 1990.
- [28] C. Wang, Y. Li, K. Peng, B. Hong, Z. Wu, and C. Sun, "Coordinated optimal design of inverter controllers in a micro-grid with multiple distributed generation units," *IEEE Trans. Power Syst.*, vol. 28, no. 3, pp. 2679–2687, Aug. 2013.
- [29] P. Nayak and A. Devulapalli, "A fuzzy logic-based clustering algorithm for WSN to extend the network lifetime," *IEEE Sensors J.*, vol. 16, no. 1, pp. 137–144, Jan. 2016.

- [30] M. Althoff and B. H. Krogh, "Zonotope bundles for the efficient computation of reachable sets," in *Proc. 50th IEEE Conf. Decis. Control Eur. Control*, 2011, pp. 6814–6821.
- [31] M. Khanabadi, Y. Fu, and L. Gong, "A fully parallel stochastic multiarea power system operation considering large-scale wind power integration," *IEEE Trans. Sustain. Energy*, vol. 9, no. 1, pp. 138–147, Jan. 2018.
- [32] L. Keyan, S. Wanxing, and L. Yun-Hua, "Research on parallel algorithm of DC optimal power flow in large interconnection power grids," in *Proc.* 8th Int. Conf. Elect. Mach. Syst., 2005, vol. 2, pp. 1031–1036.
- [33] Z. Zhang, Y. Cheng, S. Nepal, D. Liu, Q. Shen, and F. Rabhi, "A reliable and practical approach to kernel attack surface reduction of commodity OS," 2018, arXiv:1802.07062.
- [34] L. Ren et al., "Enabling resilient distributed power sharing in networked microgrids through software defined networking," Appl. Energy, vol. 210, pp. 1251–1265, 2018.
- [35] M. Althoff and D. Grebenyuk, "Implementation of interval arithmetic in CORA 2016," in *Proc. 3rd Int. Workshop Appl. Verification Continuous Hybrid Syst.*, 2016, pp. 91–105.
- [36] K. Murphy, Machine Learning: A Probabilistic Perspective. Cambridge, MA, USA: MIT Press, 2012.



Yan Li (SM'13) received the B.Sc. and M.Sc. degrees in electrical engineering from Tianjin University, Tianjin, China, in 2008 and 2010, respectively. She is currently working toward the Ph.D. degree in electrical engineering with the University of Connecticut, Storrs, CT, USA. Her research interests include microgrids and networked microgrids, formal analysis, power system stability and control, software defined networking, and cyber-physical security.



Peng Zhang (M'07–SM'10) received the Ph.D. degree in electrical engineering from The University of British Columbia, Vancouver, BC, Canada, in 2009. He is the Centennial Professor, Charles H. Knapp Chair Professor and an Associate Professor in electrical engineering with the University of Connecticut, Storrs, CT, USA. He is also the Francis L. Castleman Professor in Engineering Innovation at the University of Connecticut. He was a System Planning Engineer with British Columbia Hydro and Power Authority, Vancouver, BC, Canada. His research interests in-

clude microgrids, power system stability and control, cyber security, and smart ocean systems.

Dr. Zhang is an individual member of CIGRÉ. He is an Editor for the IEEE TRANSACTIONS ON POWER SYSTEMS and the IEEE Power and Energy Society Letters, an Associate Editor for the IEEE JOURNAL OF OCEANIC ENGINEERING, and an Associate Editor for the IEEE TRANSACTIONS ON INDUSTRIAL ELECTRONICS.



Matthias Althoff received the Diploma Engineering degree in mechanical engineering and Ph.D. degree in electrical engineering from Technische Universität München, Garching, Germany, in 2005 and 2010, respectively. He is currently an Assistant Professor in computer science with Technische Universität München. From 2010 to 2012, he was a Postdoctoral Researcher with Carnegie Mellon University, Pittsburgh, PA, USA, and from 2012 to 2013, an Assistant Professor with Technische Universität Ilmenau, Ilmenau, Germany. His research interests

include formal verification of continuous and hybrid systems, reachability analysis, planning algorithms, nonlinear control, robotics, automated vehicles, and power systems.

Meng Yue (M'03) received the B.S. degree from Xi'an Technological University, Xi'an, China, the M.S. degree from Tianjin University, Tianjin, China, and the Ph.D. degree from Michigan State University, East Lansing, MI, USA, in 1990, 1995, and 2002, respectively, all in electrical engineering. He is currently with the Department of Sustainable Energy Technologies, Brookhaven National Laboratory, Upton, NY, USA. His research interests include power system stability and dynamic performance analysis, preventive, corrective, and stabilizing control, renewable energy modeling and integration, and high-performance computing and probabilistic risk assessment applications in power systems.